Estuarine, Coastal and Shelf Science 281 (2023) 108195

Contents lists available at ScienceDirect

Estuarine, Coastal and Shelf Science

journal homepage: www.elsevier.com/locate/ecss

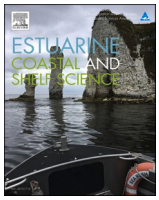

Spatial distribution of seawater carbonate chemistry and hydrodynamic controls in a low-inflow estuary

Sarah E. Bartoloni [a], Ryan K. Walter [b], Sydney N. Wewerka [b], Jolie Higgins [a], Jennifer K. O'Leary [c,d], Emily E. Bockmon [a,*]

[a] Chemistry and Biochemistry Department, California Polytechnic State University, San Luis Obispo, CA, USA
[b] Physics Department California Polytechnic State University, San Luis Obispo, CA, USA
[c] California Sea Grant, San Luis Obispo, CA, USA
[d] Wildlife Conservation Society, Mombasa, Kenya

ARTICLE INFO

Keywords:
Total alkalinity
Flushing time
Seagrass
Estuarine hydrodynamics
Hypersaline
Low-inflow estuary

ABSTRACT

Coastal and estuarine systems play an important role in the global carbon cycle and often have complex carbonate chemistry dynamics due to a multitude of biogeochemical and physical drivers. Compared to classic estuaries, mechanisms driving the distribution of carbonate parameters in low-inflow estuaries are understudied. The spatial distribution of carbonate chemistry and hydrodynamic parameters were characterized in Morro Bay, a short and seasonally hypersaline estuary on the Central California Coast, during the dry, low-inflow season to better understand in situ modifications. Sampling transects were completed in the main channel in June, August, and September of 2018, bracketing both a high and low tide on each date. Temperature, salinity, total alkalinity, and dissolved inorganic carbon all increased from the mouth to the back of the estuary, with larger values observed during the low tide. pH values decreased towards the back of the bay, and had little variation between high and low tide for June and August transects. Flushing times (estimated using a salt-budget model approach) also increased toward the back of the bay which led to hypersaline conditions. Salinity alone only explained 20–33% of observed changes in total alkalinity and 13–22% of observed changes in dissolved inorganic carbon throughout the bay. The remaining changes in total alkalinity and dissolved inorganic carbon were likely driven by biogeochemical modifications enhanced by extended flushing times, particularly in the back bay. Prior to this project, Morro Bay experienced a recent, rapid collapse of eelgrass, the major biogenic habitat. In the last four years eelgrass in Morro Bay appears to be on a recovery trajectory; therefore, this study provides a baseline whereby future studies can evaluate carbonate chemistry changes associated with potential eelgrass recovery and expansion. This study highlights the unique hydrodynamic exchange in seasonally low-inflow estuaries and its potentially large role in influencing local carbonate chemistry and ocean acidification.

1. Introduction

While anthropogenic emissions have driven an expected and measurable decrease in pH in the open ocean (Bates and Samuels, 2001; Bates, 2007; Santana-Casiano et al., 2007; Dore et al., 2009; Olafsson et al., 2010), carbonate chemistry dynamics in coastal and estuarine systems are often more complex (Borges, 2005; Hofmann et al., 2011). Biogeochemical and physical drivers can play a substantial role in the spatial distribution of carbonate chemistry in estuarine environments (Feely et al., 2010; Cai et al., 2020; Shen et al., 2020). Studies on estuarine carbonate chemistry dynamics have focused on the role of metabolic variability in estuaries (Wallace et al., 2014; Baumann and Smith, 2018), as primary production consumes dissolved carbon dioxide therefore increasing pH and decreasing dissolved inorganic carbon (DIC). This includes both seasonal (Reum et al., 2014; Carstensen et al., 2018) and diel variability in biological productivity (Challener et al., 2016; Cyronak et al., 2018), which typically produce strong correlations between dissolved oxygen and pH. Other important drivers of carbonate chemistry dynamics include the remineralization of organic matter (Feely et al., 2010) and eutrophication (Wallace et al., 2014) which can amplify extremes when microbial respiration dominates. Eutrophication can also drive ecosystem metabolism by stimulating primary production

* Corresponding author.
E-mail address: ebockmon@calpoly.edu (E.E. Bockmon).

https://doi.org/10.1016/j.ecss.2022.108195
Received 22 December 2021; Received in revised form 16 December 2022; Accepted 20 December 2022
Available online 23 December 2022

(Borges and Gypens, 2010; Cotovicz et al., 2015). Further, anaerobic respiration (Cai and Wang, 1998; Abril et al., 1999; Cai et al., 2017), denitrification, (Crosswell et al., 2020), and sulfate reduction (Borges, 2005; Bouillon et al., 2007; Krumins et al., 2013; Sippo et al., 2016; Carstensen et al., 2018) can all play a role in carbonate chemistry dynamics depending on the estuarine conditions and ecosystem. Estuarine systems are also particularly susceptible to fluctuations in pH due to variable freshwater inputs which reduces buffering capacity by decreasing TA relative to the open ocean (Miller et al., 2009; Hu et al., 2015). Physical controls such as the tidally driven mixing of fresh and salt water (Feely et al., 2010; McCutcheon et al., 2019; Omarjee et al., 2020), resuspension of carbonate sediments (Abril et al., 2004), flux of TA and DIC from submarine groundwater (Murgulet et al., 2018), and air-sea gas exchange (Bates and Samuels, 2001), can shape estuarine carbonate chemistry.

Most estuarine carbonate chemistry characterizations have occurred in larger estuaries with substantial freshwater input (Frankignoulle et al., 1998; Borges, 2005; Cai et al., 2020), where TA is driven by conservative mixing (Carstensen et al., 2018). In these systems, TA is most often positively correlated with salinity, and thus typically decreases towards the back of an estuary where freshwater discharge occurs, although some systems are subject to freshwater inputs with high TA (e.g., Cantoni et al., 2012; McGrath et al., 2016). Submarine groundwater discharge can also be a source of TA and DIC to estuarine environments, especially when riverine input is low (Cyronak et al., 2013; Murgulet et al., 2018). Calcification and dissolution have been shown to control seasonal variability of the spatial distribution of TA in some larger estuaries (Hu et al., 2015; Carstensen et al., 2018), while ecosystem responses to nutrient inputs (Shen et al., 2019), eutrophication (Kemp et al., 2005; Borges and Gypens, 2010), and hypoxia (Li et al., 2016; McCutcheon et al., 2019) also often significantly modify the carbonate chemistry in these larger systems. In large estuarine systems such as Puget Sound and Chesapeake Bay, pH has been found to increase (and DIC decrease) toward the ocean at the surface, decrease with depth, and is largely controlled by metabolic processes (Feely et al., 2010; Brodeur et al., 2019). Few studies have analyzed the spatial distribution of carbonate chemistry in small and shallow estuaries (Yao and Hu, 2017; Baumann and Smith, 2018; Li et al., 2020) or estuaries with seasonally low freshwater inputs (Cyronak et al., 2018; Paulsen et al., 2018; Cotovicz et al., 2021, 2022). These systems may be differently affected by acidification and other natural- and human-induced modifications, particularly those with low freshwater input, since they have been shown to be hydrodynamically controlled and sensitive to a host of natural and anthropogenic processes (Schettini et al., 2017; Walter et al., 2018a).

In arid regions and in Mediterranean climates during the dry season, most estuaries receive little to no precipitation or freshwater inputs and are called low-inflow estuaries (LIEs; Largier et al., 1997; Nidzieko and Monismith, 2013; Schettinit et al., 2017; Walter et al., 2018a). One of the defining characteristics of LIEs is a long residence time relative to the time scale of evaporative surface fluxes, thereby leading to systems where evaporation is a major control on estuarine hydrodynamics. Moreover, in LIEs, longitudinal density gradients and vertically sheared circulation are weak such that longitudinal exchange and mixing is primarily controlled by tidal motions, contrasting with the two-layer estuarine circulation (i.e., gravitational circulation) observed in "classical" estuaries with significant freshwater input (Largier et al., 1997; Largier, 2010). In these low-inflow systems, evaporative losses can exceed freshwater inputs leading to hypersaline basins, increased residence times (via decreased diffusion), and the development of longitudinal zones with distinct water mass properties (Largier, 2010; Buck et al., 2014; Walter et al., 2018a). For example, long residence times can increase the degree of pH variability due to local remineralization and primary production (Omarjee et al., 2020). However, CO_2 flux from a low-inflow estuarine system has been shown to be much smaller than in a riverine dominated system, mostly driven by seasonal temperature changes as well as production and remineralization processes in the adjacent salt marsh (Jiang et al., 2008). Understanding how these characteristics and the dynamics of LIEs mediate changes in biogeochemistry has implications for estuarine ecosystems and could contribute to management of these estuaries under future climate change and ocean acidification scenarios.

In this study, we investigate the role that estuarine hydrodynamics play in shaping spatial distributions of carbonate chemistry in a small, low-inflow estuary (Morro Bay, California USA). This is the first study to evaluate carbonate chemistry in Morro Bay and an opportunity to study carbonate chemistry dynamics across a gradient of physical conditions and processes. This study will allow for a better predictive capacity of estuarine processes in similar LIE systems globally. Moreover, Morro Bay has experienced large-scale eelgrass declines over the past decade with a loss of >95% of its eelgrass, with a decline from 139 ha (344 acres) in 2007 to <6 ha (15 acres) in 2017 (Walter et al., 2018a, 2020; O'Leary et al., 2021). Recently, there are signs that eelgrass may be on a recovery trajectory in Morro Bay. Eelgrass can modify water column carbonate chemistry by drawing down seawater inorganic CO_2 through high rates of primary production (Duarte et al., 2010; Unsworth et al., 2012; Hendriks et al., 2014) and has been studied for its potential to mitigate local acidification impacts on nearby calcifying organisms (Unsworth et al., 2012; Abe et al., 2022). A better understanding of the processes that govern spatial and temporal variability of carbonate chemistry dynamics in hypersaline estuarine systems like Morro Bay is needed, with important implications for how these systems will respond to emerging threats including ocean acidification (e.g., Kroeker et al., 2013), habitat and biodiversity loss (Worm et al., 2006; Sippo et al., 2016; Hall-Spencer and Harvey, 2019), and eutrophication (Malone and Newton, 2020).The results presented here are therefore also an important baseline of carbonate chemistry dynamics in a system under transition, allowing future evaluation of changes in the carbonate chemistry as eelgrass recovers.

2. Study site and methods

2.1. Site description

Morro Bay is a short, shallow estuary that is characterized by mixed semidiurnal tides (dominated by M_2 and K_1 tidal constituents) and located along the Central California Coast, USA (Fig. 1). It is home to a

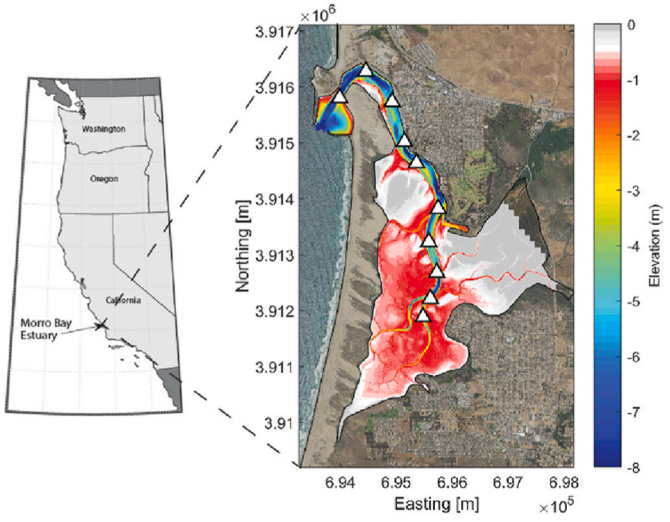

Fig. 1. Morro Bay site map located along the Central California Coast, USA. Elevation relative to mean sea level shown in the estuary, along with the locations of the ten profiling and sampling locations along the main channel (triangles) with station 1 located at the bay mouth.

major fishing port, two aquaculture facilities (oysters), and features a diverse population of invertebrates, fish, and birds (native and migratory). The Mediterranean-climate estuary is typified by an extended dry season (~April to October) with little to no precipitation and freshwater inputs, and a shorter wet season (~November to March) with episodic precipitation and freshwater inputs (Fig. S1; Walter et al., 2020). The main tidally-forced channel of the estuary gets progressively shallower going from the mouth to the back bay over a distance of roughly 6.5 km (Fig. 1). During the summer dry season, strong gradients in environmental conditions persist throughout the estuary. In particular, the middle and back portions of the bay are characterized by elevated temperatures (hyperthermal), increased salinities (hypersaline), higher turbidities, and large flushing times relative to the mouth (Walter et al., 2018a). The main subtidal channel is flanked by intertidal mudflats, which historically supported large expanses of eelgrass (*Zostera marina*) meadows, prior to a recent decline (cf. Walter et al., 2018a) that led to widespread erosion (Walter et al., 2020) and changes to fish populations (O'Leary et al., 2021).

2.2. Sampling collection

To better understand spatial variability in environmental conditions and carbonate chemistry in the estuary, boat-based transects comprised of ten sampling stations spanning the bay were completed on three separate days throughout the summer dry season. Transects were completed on June 28, August 9, and September 7, 2018, which are hereafter referred to as Early, Mid, and Late Summer sampling days. On each sampling day, two bay-wide transects were carried out, with each transect spanning either a high or low tide (i.e., with the start and end times within 1 h of the published high or low tide, respectively – see Table 1). All high tide sampling occurred during the lower high water at similar tidal heights, while all low tide sampling took place during the higher low water at similar tidal heights, respectively (see Table 1). Each high and low tide transect consisted of 10 sampling locations (Stations 1–10, where Station 1 is at the bay mouth and Station 10 is near the bay head) along the main channel (Fig. 1). Stations were sampled following the direction of each respective tide (e.g., starting at Station 1 for high tide and Station 10 for low tide). High tides were consistently earlier in the day and low tides later in the day (see Table 1). Sampling dates were designed to bracket seasonal variability during the summer dry season and to observe high and low tide spatial variability during similar daylight conditions. At each sampling station, discrete water samples were collected via Niskin at an average depth of 2.5 m. The June high and low tide transects were too shallow at Stations 9 and 10 so samples were collected at 1.5 m. All samples were immediately preserved with 120 μL of a saturated $HgCl_2$ solution following Dickson et al. (2007). Vertical profiles of conductivity (salinity), temperature, and pressure (depth) were also collected using a Sea-Bird Scientific 19+ profiling conductivity-temperature-depth (CTD) instrument sampling. The CTD sampled at 4 Hz continuously throughout the water column and data were vertically-averaged in 0.25 m bins.

2.3. Carbonate sample analysis

Samples were analyzed for TA and DIC within two months of the corresponding transect. Samples did not undergo filtration before analysis. TA was measured via automated open-cell titration (Dickson et al., 2003) and DIC was determined using automated acidification and a non-dispersive infrared gas analyzer (NDIR), as described in Bockmon and Dickson (2015). Instruments were calibrated using CO_2 seawater Certified Reference Materials (CRM) from the Dickson Laboratory at Scripps Institution of Oceanography, UC San Diego. The uncertainty of the measurements is estimated to be ±3 μmol kg^{-1} for TA and ±4 μmol kg^{-1} for DIC. Three samples were excluded from data analysis and interpretation due to analysis error. Sample pH (total scale), calcium carbonate saturation state of aragonite (Ω_A), and the partial pressure of carbon dioxide (pCO_2) were calculated at in situ temperature and pressure using sample TA and DIC via MATLAB CO2SYS v1.1 (van Heuven et al., 2011). Dissociation constants from Millero (2010), KSO_4 constant from Dickson (1990), and total borate value from Lee et al. (2010) were used in this calculation, with silicate and phosphate concentrations assumed to be zero.

2.4. Flushing time estimates

To quantify flushing times throughout the bay, a subtidal longitudinal salt balance approach for hypersaline estuaries was utilized following Largier et al. (1997), Largier (2010), and Walter et al. (2018a), which we briefly outline here. During the low-inflow dry season, precipitation and riverine freshwater inflows are negligible (e.g., Fig. S1) such that changes in salt content are dominated by diffusive salt fluxes and evaporation,

$$\frac{\partial S}{\partial t} = \frac{\partial}{\partial x}\left[K_x \frac{\partial S}{\partial x} + \frac{Ex}{H} S\right], \tag{1}$$

where $S(x,t)$ is the tidal average salinity, $E(t)$ is the evaporation rate, $H(x)$ is the water depth, x is the longitudinal distance from the estuary head (i.e., $x = 0$ at the head, with positive x seaward from the head), and $K_x(x,t)$ is the longitudinal salt diffusivity. Assuming a dry-season steady-state, and scaling the longitudinal diffusivity according to the Prandtl mixing length theory (e.g., $K_x = kx^2$, where k is a constant determined from the model fit described below and both the velocity and length scales of tidal motion scale with x since longitudinal dispersion is dominated by tidal motions in the absence of density-driven vertical exchange; Largier et al., 1997), the following analytical expression is obtained from Equation (1) for the salinity decrease with distance from the head:

$$S = S_o \left(\frac{x}{L}\right)^{-\frac{E}{kH}}, \tag{2}$$

where S_o is the ocean salinity, H is the average channel depth, and L = 6.0 km is the approximate channel length. Evaporation was calculated as

$$E = Q_L / (L_e \rho_w), \tag{3}$$

Table 1
Sampling dates, tidal information, and time of transect (local time; Pacific Daylight Time).

		Date	Tide Height (m Mean Lower Low Water)	Time of Peak Tide	Time of Transect
High Tide	*Early*	Jun 28, 2018	1.20	12:12	11:13–13:12
	Mid	Aug 9, 2018	1.35	9:54	9:01–10:54
	Late	Sept 7, 2018	1.44	9:30	8:29–10:10
Low Tide	*Early*	Jun 28, 2018	0.80	16:30	15:34–17:23
	Mid	Aug 9, 2018	0.77	14:36	13:42–15:14
	Late	Sept 7, 2018	0.64	14:42	13:32–15:02

where Q_L is the latent heat flux calculated using the bulk formula in Rosenfeld et al. (1994) (see also Suanda et al., 2011; Walter et al., 2017), L_e is the latent heat of evaporation, and ρ_w is the density of water. Meteorological data (15 min intervals) were obtained from a long-term monitoring site located near Station 9 (see Walter et al., 2018a; https://data.cencoos.org/?&sensor_version=v2#metadata/57163/station/data).

For each of the three sampling days, using the depth-averaged salinity at each of the ten sampling locations averaged across the high and low tide transects, and an estimate of evaporation over the previous thirty days, the data were fit to Equation (2) using a nonlinear least squares regression to determine the constant k. Following this, flushing times, or the time needed to completely diffuse the hypersalinity out of the basin at different spatial locations, were estimated from

$$\tau_{flush} = \frac{(S - S_o)x}{-K_x \frac{\partial S}{\partial x}}, \tag{4}$$

where $\frac{\partial S}{\partial x}$ was determined from Equation (2). The flushing time estimates were also comparable to residence time estimates (e.g., approximate age of water parcel) computed at discrete points using a bulk (Lagrangian) salt balance:

$$\tau_{res} \sim \frac{(S - S_o)H}{ES_{avg}}, \tag{5}$$

where $S_{avg} = \frac{S+S_o}{2}$ is a measure of the Lagrangian average salinity. Further details on the above flushing time methodology can be found in Largier et al. (1997), Largier (2010), and Walter et al. (2018a).

2.5. Calculation of contributions to TA and DIC

Calculations were performed to quantify the contribution of salinity (e.g., the development of hypersaline conditions due to long flushing times expected for a LIE estuary) to the variability of TA throughout the bay at low tide. First, the expected TA due to the conservative modification of TA by salinity was calculated at each station using methods similar to Jiang et al. (2014) and Cotovicz et al. (2021) (Equation (6)). The expected change in TA due to salinity ($\Delta TA_{salinity}$), relative to the mouth was calculated at each station and sampling date as:

$$\Delta TA_{salinity} = TA_m * \left(\frac{S_z}{S_m}\right) - TA_m, \tag{6}$$

where S denotes salinity, subscript z denotes a particular sampling station, and subscript m denotes the mouth station (i.e., Station 1). Finally, the percent contribution of TA increase due to salinity was then determined by calculating the fraction of expected change in TA as a result of salinity over the total observed change in TA at each station:

$$\%\ \text{Contribution} = \frac{\Delta TA_{salinity}}{TA_z - TA_m} * 100. \tag{7}$$

This calculation was repeated for DIC:

$$\Delta DIC_{salinity} = DIC_m * \left(\frac{S_z}{S_m}\right) - DIC_m, \tag{8}$$

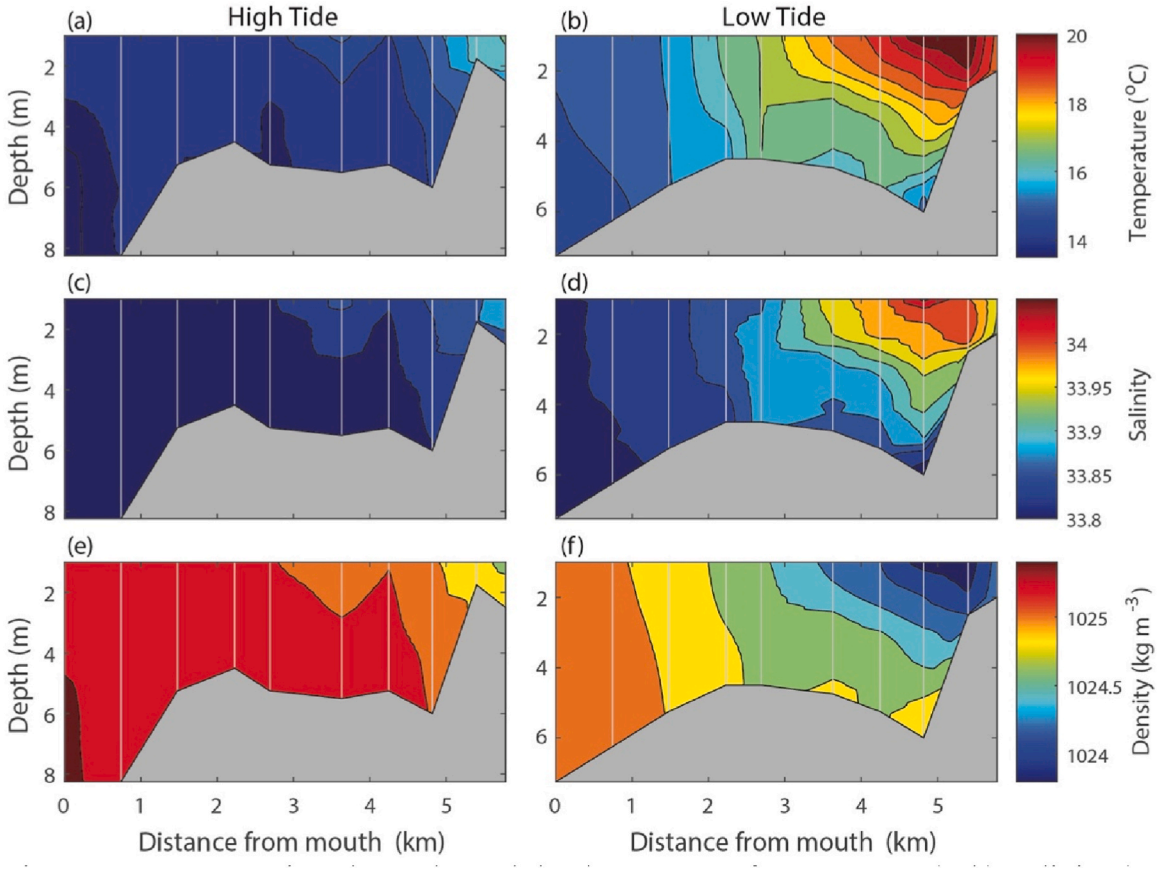

Fig. 2. Representative along-channel depth contours of temperature (a, b), salinity (c, d), and density (e, f) from Early Summer, during the high (left, panels a, c, e) and low (right, panels b, d, f) tides. For each respective parameter, the same color bar is used for high and low tide for comparison. The vertical grey lines denote profiling locations (Stations 1 and 10 are at the left and right edges of plot, respectively), and the maximum depth of each profile was used to create the shaded grey bathymetry for each respective tide. Contour levels generated from linearly interpolating profile data are shown in increments of 0.5 °C, 0.025, and 0.2 kg m^{-3}, for temperature, salinity, and density, respectively. (For interpretation of the references to color in this figure legend, the reader is referred to the Web version of this article.)

$$\% \text{ Contribution} = \frac{\Delta DIC_{salinity}}{DIC_z - DIC_m} * 100. \quad (9)$$

High tide calculations of percent contribution to TA and DIC were excluded due to the nearly constant salinity observed throughout the bay, but the changes in TA and DIC relative to bay mouth (Station 1; Δ TA and Δ DIC) were calculated, at high and low tide, to observe how different biogeochemical processes modify carbonate chemistry.

3. Results

3.1. Temperature and salinity variability and flushing times

All three sampling days showed similar vertical and horizontal spatial patterns in temperature, salinity, and density throughout the estuary (Early Summer depth contours are highlighted in Fig. 2, Mid and Late Summer depth contours are shown in Figs. S2 and S3, and parameters at an average depth of 2.5 m for all transects are shown in Fig. 3 a–f and Table S1). During high tide, colder and slightly less saline waters are observed throughout the estuary, with only small spatial differences observed in the very back portions of the estuary. During low tide, substantially warmer and slightly more saline back bay waters are observed throughout most of the estuary, except at the mouth which maintains similar conditions to those observed during the high tide. Thus, the middle region of the bay acts as a transition zone between the mouth and the back bay water masses, with minimal exchange between the longitudinal regions. Despite the hypersaline conditions in the back bay, these waters are still less dense compared to the mouth due to the significantly higher temperatures. The estuary is generally well mixed in the vertical except in the very back portions of the bay which exhibits minimal vertical density stratification.

Flushing time estimates displayed similar spatial patterns across all sampling dates (Fig. 4). As expected for a hypersaline system, flushing times were on the order of hours to days near the mouth and increased substantially in the back bay with flushing times of over 13 days in the Early Summer and approximately 20 days in the Mid and Late Summer. The smaller flushing times observed in Early Summer are likely due to the decreased salinity gradient (e.g., level of hypersalinity) observed across the bay (Fig. 3 d–f).

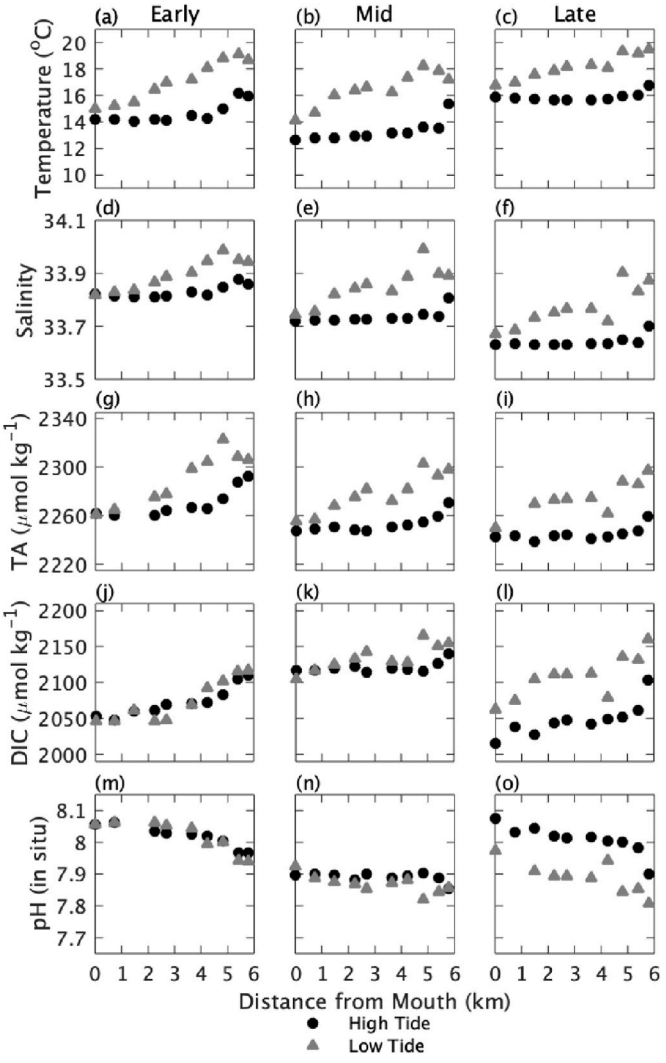

Fig. 3. Data from all three transects separated by sampling date for Early Summer (left), Mid Summer (middle), and Late Summer (right), for both low (grey triangle) and high (black circle) tide. Temperature (a–c) and salinity (d–f) were collected by CTD. TA (g–i) and DIC (j–l) were measured from bottle samples within two months of sample collection. pH (m–o) reported on the total scale at in situ temperature was calculated using CO2SYS for MATLAB. All data are from an average of 2.5 m depth.

3.2. Carbonate chemistry variability

Temporal variations between high and low tide varied among the carbonate parameters (TA, DIC, and pH), but remained consistent across sampling days. TA displayed the largest magnitude change between high and low tide across all sampling days. On average, the TA at low tide increased by 20 ± 15, 26 ± 12, and 25 ± 19 relative to the high tide for Early, Mid, and Late Summer, respectively (Fig. 3 g–i). At bay mouth, low tide TA was −1, 8, and 7 μmol kg^{-1} higher than high tide TA for Early, Mid, and Late Summer respectively (Fig. 3 g–i). At the farthest back bay station, low tide TA was 14, 28, and 37 μmol kg^{-1} higher than the corresponding high tide samples. Temporal differences between low and high tide TA values increased toward the back bay stations. DIC and pH did not display significant changes between low and high tide for Early and Mid Summer but large variations between tides were present in Late Summer at all stations throughout the bay. DIC at low tide increased by 1 ± 14, 14 ± 17, 63 ± 16 μmol kg^{-1} averaged across all stations for Early, Mid, and Late Summer, respectively (Fig. 3 j–l). The station at the bay mouth decreased at low tide compared to high tide by 7 and 12 μmol kg^{-1} for DIC in Early and Mid Summer (Fig. 3 j,k), while in Late Summer, the mouth station at low tide was 48 μmol kg^{-1} higher than high tide (Fig. 3 l). Additionally, DIC at the farthest back bay station increased at low tide by 7, 15, and 57 μmol kg^{-1} for Early, Mid, and Late Summer, respectively. Low tide and high tide pH did not differ in Early or Mid Summer with a difference of 0.00 ± 0.02 and of 0.02 ± 0.03 units across all stations (Fig. 3 m, n). For Late Summer, low tide pH

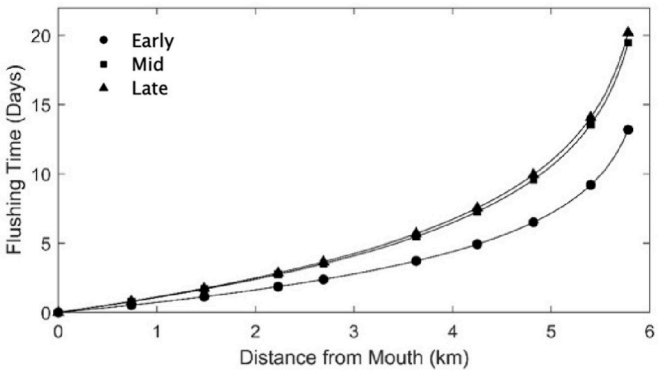

Fig. 4. Estimated flushing time as a function of distance from the mouth with the location of profiling and sampling shown for Early (circles), Mid (squares), and Late (triangles) Summer.

was an average and 0.12 ± 0.03 units lower than high tide values (Fig. 3 o). Overall, TA displayed consistent differences between high and low tide across all respective sampling dates while DIC and pH only had significant variations between high and low tide in Late Summer.

Carbonate chemistry parameters displayed substantial spatial differences throughout the bay. TA values consistently increased from bay mouth to back bay with the farthest back bay station being 45, 43, and 47 μmol kg^{-1} higher at low tide and 30, 23, and 17 μmol kg^{-1} higher than bay mouth at high tide for Early, Mid, and Late Summer, respectively.

DIC also increased towards the back bay across all sampling dates. Low tide DIC was 70, 50, and 97 μmol kg^{-1} higher while high tide DIC was 56, 23, and 88 μmol kg^{-1} higher at the farthest back bay station compared to the bay mouth. Additionally, pH in the back bay decreased relative to bay mouth for low and high tide respectively by 0.12 and 0.09 in Early Summer, 0.04 and 0.07 in Mid Summer, and 0.17 and 0.17 in Late Summer. All parameters displayed consistent trends in spatial variability across all sampling dates with TA and DIC values increasing toward the back bay and pH decreasing toward the back bay.

Calculated aragonite saturation state (Ω_A) values displayed minimal spatial and tidal variability with values in the range of 1.5–2.6 (Table S1, Fig. S4). In addition, calculated pCO_2 values were typically in the range of 385–700 μatm with the highest values in the back bay at low tide in the Late Summer (Table S1, Fig. S4).

During the low tides, when TA gradients were strongest across the bay, the percent contribution of salinity to TA changes calculated using Equations (6) and (7) and averaged across all ten stations was 20 ± 4%, 33 ± 6%, and 28 ± 6% for the Early, Mid, and Late Summer transects, respectively. The percent contribution of salinity to DIC increase at low tide was 16 ± 5%, 22 ± 9%, and 13 ± 4% for Early, Mid, and Late Summer (Equations (8) and (9)). Therefore, 67–80% of the observed increase in TA and 78–87% of the observed increase in DIC relative to the mouth are due to other contributions. Fig. 5 highlights expected changes in TA and DIC given a conservative relationship with salinity and increases due to evaporation. The evaporation pathway was calculated using $\Delta TA_{salinity}$ and $\Delta DIC_{salinity}$ from Equations (6) and (8). Nearly all observed low tide TA and DIC values were above this evaporation pathway line. During high tide there were only small changes in salinity throughout the bay highlighting that observed changes in TA and DIC are not due to evaporation (Fig. 5).

4. Discussion

4.1. Comparison with other systems

Strong spatial gradients were consistently observed in Morro Bay across all three summer sampling periods with increases in temperature, salinity, TA, and DIC, and decreases in pH, going from the mouth to the back bay. At the bay mouth (Station 1), the temperature, salinity, TA, DIC, and pH varied across all three sampling dates (Fig. 3) with values reflecting expected variability in the composition of seawater along the CA coast during the upwelling season which brings cold, high DIC and

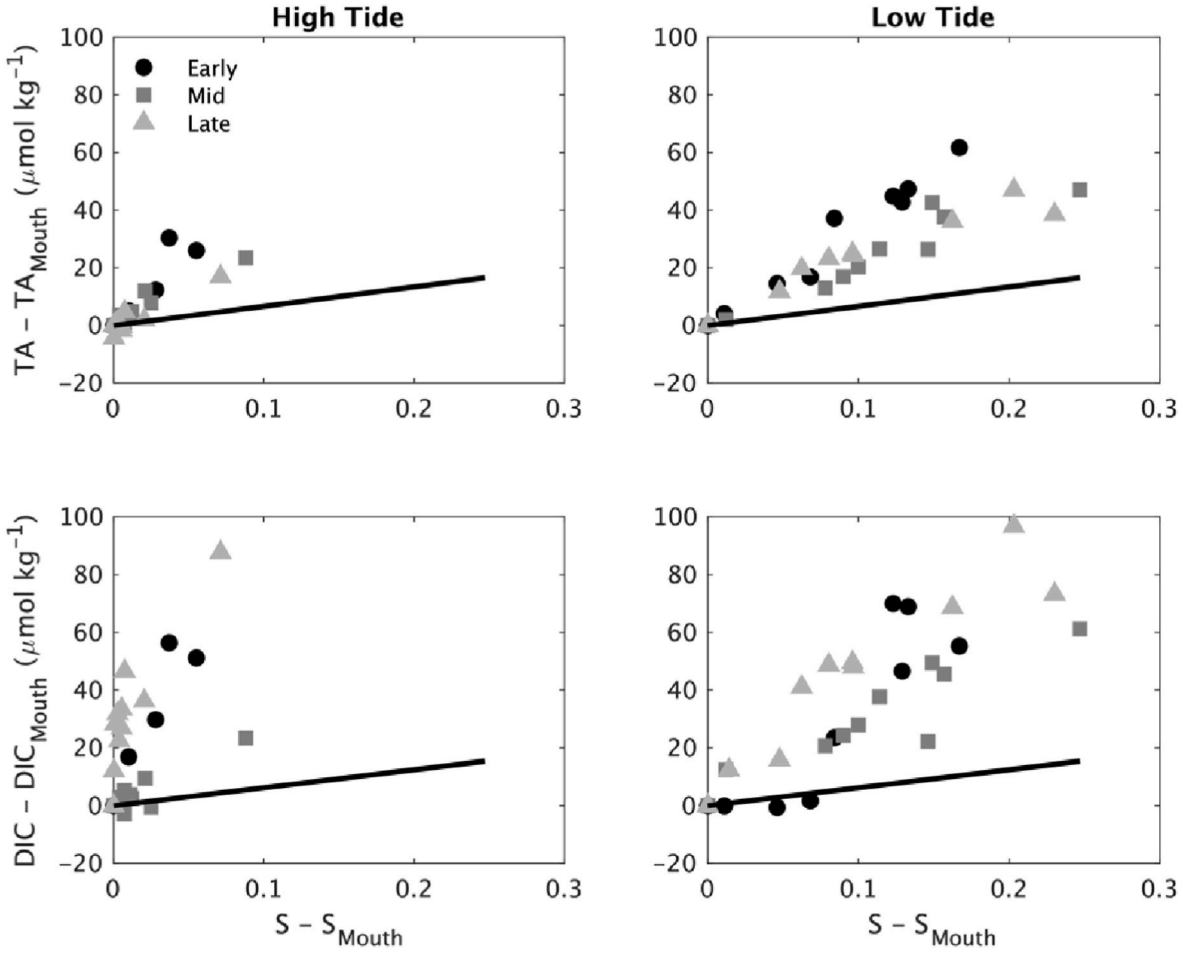

Fig. 5. Changes in TA (top) and DIC (bottom) as a function of change in salinity at high (left) and low tide (right), all relative to the bay mouth and separated by sampling date: Early (black circles), Mid (dark grey squares), and Late (light grey triangles) Summer. Changes due to evaporation are represented by the expected change in TA and DIC due to its conservative relationship with salinity (black line). Data points below this line can be fully explained by evaporation. The changes in parameters were calculated for each transect, where bay mouth values were subtracted from all other stations to represent the change throughout the bay.

low pH waters to the surface (Hauri et al., 2009; Alin et al., 2012; Gruber et al., 2012; Walter et al., 2018b). Despite the variations in source water entering at the bay mouth across the sampling periods, spatial patterns of TA were consistent across all sampling days while DIC and pH showed similar patterns in Early and Mid Summer transects. Similar spatial patterns across the bay, despite varied characteristics of water entering at the bay mouth, indicate consistent water modification processes within the estuary. These include evaporative processes increasing salinity towards the bay head and increased temperatures due to long flushing times and shallow waters as is typical of LIEs during the dry summer season.

Despite the ubiquity of single main channel low-inflow intertidal estuarine systems in Mediterranean climates, the sparsity of carbonate chemistry literature in these systems means there is not a directly comparative system (see e.g., Hu et al., 2015; Sippo et al., 2016; Cyronak et al., 2018; Paulsen et al., 2018; Crosswell et al., 2020; Cotovicz et al., 2022). The closest comparative study investigated spatial gradients in pH, DIC, TA, and dissolved oxygen (DO) in Mission Bay, CA, a highly modified and enclosed urbanized estuarine system with low freshwater inputs, using daily discrete measurements spanning a grid of seagrass meadows within the bay over a two-day period in the late fall (Cyronak et al., 2018). Unlike Morro Bay, the Mission Bay system does not have a distinct main channel and its bay wide spatial distributions of carbonate chemistry have not yet been reported. pH in the seagrass meadow in Mission Bay exhibited spatial variability which was greater than diel variability, with the largest spatial variability observed at low tide. Throughout Mission Bay, pH values were rarely lower than the adjacent oceanic source water. In contrast, this study consistently found pH in the back portions of Morro Bay to be lower than the mouth source waters, indicating different biological drivers modifying pH between the two estuaries. For example, Mission Bay sample sites were within a seagrass meadow while Morro Bay's seagrass population was small at the time of this study. In both Mission Bay and Morro Bay, the spatial variability of TA was at least partially driven by strong tidal forcing and changes in salinity. Another study examined the temporal and along-channel spatial distribution of carbonate chemistry of San Dieguito Lagoon, a shallow (<2 m), single channel salt marsh lagoon located north of San Diego, CA, by collecting discrete samples in the morning hours on four days spanning from the late summer to late fall (Paulsen et al., 2018). Changes in carbonate chemistry before, during, and after a large precipitation event were measured in this study. For measurements made in late summer prior to precipitation and freshwater input — the time period most applicable to the summer dry season in the current study — this system has a residence time of 4–6 days, but did not display hypersaline conditions. Similar to Morro Bay, DIC and TA were found to increase towards the back bay, while pH decreased. Although San Dieguito Lagoon had similar spatial patterns to those observed in Morro Bay, the different salinity gradients in these two systems indicate a difference in hydrodynamics which may alter drivers of carbonate chemistry variability.

4.2. Spatial variability

In Morro Bay, the observed increase in TA towards the back bay was partially driven by the evaporative fluxes in that region coupled with long flushing times that led to hypersaline conditions (Equations (6) and (7)). But the relationship between changes in TA and salinity (Fig. 5), also reveals that TA increases toward the back bay beyond what is expected by evaporation alone and 67–80% of the observed increase in TA at low tide is not a result of the increase in salinity, but rather other biogeochemical processes. The observed long flushing times in the back bay thus likely causes both the increase in salinity due to evaporation as well as accumulation of TA due to other processes. Long flushing times (observed here and in other LIEs) are expected to modify the carbonate chemistry of a system by extending the time over which various biological and chemical processes can occur, including photosynthesis,

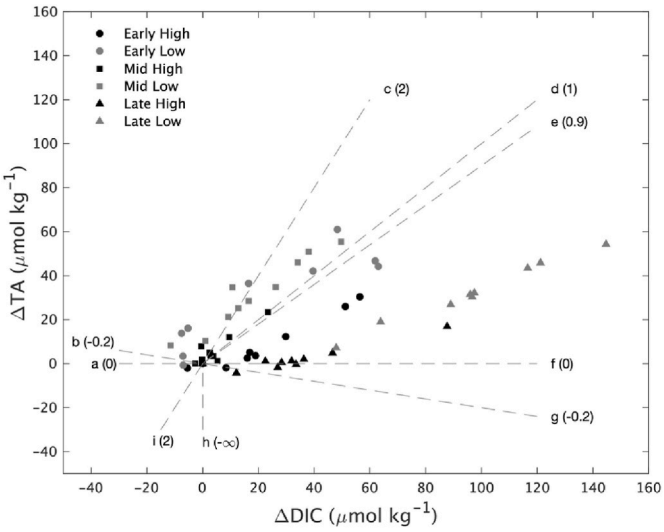

Fig. 6. ΔTA versus ΔDIC within the Morro Bay estuary separated by high (black) and low (grey) tide and for Early (circles), Mid (squares), and Late (triangles) summer. Dotted lines indicate how different biogeochemical processes will lead to changes in ΔTA and ΔDIC with fixed stoichiometric ratios (Sippo et al., 2016; Liu et al., 2017): (a) CO_2 release, (b) photosynthesis, (c) calcium carbonate dissolution, (d) sulfate reduction, (e) denitrification, (f) CO_2 invasion, (g) aerobic respiration, (h) nitrification/sulfide oxidation, and (i) calcium carbonate precipitation. The numbers in parentheses with each process indicate the slope of the line.

respiration, dissolution of carbonate minerals, and sediment redox reactions (Omarjee et al., 2020). It is possible that the increased TA (and DIC) in the back portions of the bay is driven by dissolution of carbonate material over the longer flushing times, but this is unlikely since the bay water column is super-saturated with respect to Ω_A (values > 1.5) and stoichiometric ratios of Δ TA and Δ DIC (shown in Fig. 6) confirm calcium carbonate dissolution is not a significant contributor. However, calcium carbonate dissolution may be taking place in the sediment if pore waters become undersaturated with respect to Ω_A (values < 1) (Fig. 6 c). Benthic denitrification and sulfate reduction can also contribute to water column TA and DIC (Fig. 6d and e; Cai and Wang, 1998; Abril et al., 1999; Wolf-Gladrow et al., 2007; Cai et al., 2017; Carstensen et al., 2018; Crosswell et al., 2020). Given this, it is possible that the loss of eelgrass in Morro Bay prior to the study, and the resulting change to bay geomorphology through increased erosion and sediment resuspension (e.g., Walter et al., 2018a, 2020), could be contributing carbonate derived in the sediment to the water column. Another potential source of modification to TA is the presence of oyster farms in the middle bay. Oysters form their shells through calcification by the uptake of calcium (Ca^{2+}) and bicarbonate ions (HCO_3^-) from surrounding seawater which lowers TA (Wolf-Gladrow et al., 2007). Oysters are therefore unlikely to be the cause of the observed increase in TA in the middle bay relative to bay mouth and this uptake is not supported by modifications to ΔTA and Δ DIC shown in Fig. 6. Unquantified organic alkalinity has also been identified as a contributor to measured alkalinity (Fong and Dickson, 2019; Kerr et al., 2021) particularly in coastal waters (Song et al., 2020), and has been shown to be in high concentration in estuarine sediments (Lukawska-Matuszewska et al., 2018). This organic contribution to alkalinity is included in our measured TA value and possibly contributes to the observed increased in TA in the back bay at low tide. Nutrient loads from unquantified freshwater inputs are a potential source of TA in the back bay (Borges and Gypens, 2010; Wallace et al., 2014; Shen et al., 2019), but is unlikely to be a substantial contributor since measurements took place during the dry season (see also Fig. S1) and hypersaline conditions were consistently observed. However, this study does not account for submarine groundwater

discharge which could contribute to elevated TA and DIC values in the back bay and at low tide (Murgulet et al., 2018).

Spatial gradients of DIC were consistent over this study with DIC elevated in the back bay relative to the mouth. Only 13–22% of the increase in DIC in this study is explained by salinity increase due to evaporation (Equations (8) and (9), Fig. 5). At low tide, DIC values have a greater displacement from the evaporation pathway in comparison to low tide TA (Fig. 5), indicating that less of the signal is due to evaporation (and therefore salinity). 78–87% of the increase in DIC values from bay mouth to back bay cannot be explained by its relationship to salinity. Seawater at nearly all stations had elevated pCO_2 relative to the atmosphere throughout the summer months, therefore the bay is a source of CO_2 to the atmosphere (Fig. S4). This also indicates that the spatial gradient of accumulated DIC in the back bay is not a result of atmospheric CO_2 intrusion during the long flushing times. Instead, the increases in DIC in the back bay are likely a result of respiration of organic matter (Fig. 6 g) with DIC spatial trends largely controlled by long flushing times which allow for an accumulation of biological modifications. Net aerobic respiration in the bay may be due to the lack of eelgrass in the estuary at the time of this study and the presence of two commercial oyster farms, although further work is needed to corroborate this hypothesis.

pH consistently decreased from bay mouth to back bay for all sampling dates and lowest values were observed at low tide. In the back bay, we observed the highest values of temperature, salinity, TA, and DIC. Increasing temperature of seawater leads to a decrease in pH while elevated TA acts to buffer against large pH changes (Jiang et al., 2019). Additionally, increasing water temperature leads to a decrease in the solubility of aqueous CO_2 which can result in outgassing of CO_2 from the seawater to the atmosphere. Outgassing of CO_2 leads to a decrease in DIC and pCO_2 and an increase in pH and Ω_A (Feely et al., 2012). Temperature has cancelling effects on pH given the decrease in pH with increasing temperature and the increase in pH with additional outgassing and therefore is likely not the driver of decreased pH in the back bay. Despite the increased buffering capacity of the back bay, we still see a decrease in pH from bay mouth to back bay, although if TA were not elevated in the back bay, we would expect to see a larger decrease in pH. Observed pH in the back bay is likely due to accumulated respiration which would lead to elevated dissolved CO_2, DIC, pCO_2 and decreased pH and Ω_A.

4.3. Temporal variability

Temperature, salinity, and TA all had consistent tidal variability with higher values observed at low tide and lower values observed at high tide. Elevated temperature, salinity, and TA at low tide are partially a result of the bay hydrodynamics that produced hypersaline conditions in Morro Bay during the summer sampling period. When oceanic water enters the bay mouth at high tide, bay wide salinity and TA values lower and become more spatially consistent reflecting the characteristics of the open ocean water (Fig. 5). Oceanic water with lower temperature, salinity, and TA dominates the estuary during high tide, while highly modified, hypersaline bay waters with high temperature, salinity, and TA dominate at low tide (Fig. 3).

Surprisingly, no differences were observed in DIC and pH through the day (high tides were sampled in the morning hours and low tides in the late afternoon – see Table 1) for the Early and Mid Summer transects. It is expected that daytime photosynthesis will decrease DIC and increase pH, while opposite trends are observed during night due to respiration. The small differences in carbonate chemistry from the morning high tide to the afternoon low tide, during Early and Mid Summer, can be explained by the combination of diel cycles of biological activity and tidally driven influences on carbonate chemistry. At the afternoon low tide, the concentration of DIC is likely being driven down by biological uptake, while at the morning high tide, it is likely elevated due to overnight respiration. In the Late Summer, the lowest DIC and highest pH values were observed at high tide (corresponding to morning hours) which is inconsistent with the previous summer months and expected diel variability. Although the source of this anomaly is unknown, spatial trends in DIC and pH still indicate a persistent pattern of increased CO_2 in the back bay due to increased flushing times. Additionally, this study is limited by a lack of chlorophyll and dissolved oxygen data which would help to quantify primary production and respiration throughout the study along with any temporal or spatial variations. Although DIC and pH do not vary between high and low tide in Early and Mid Summer, surely diel cycles of net respiration and primary production still play a role in controlling estuarine carbonate chemistry along with the influence of long flushing times throughout the bay.

4.4. Ecological considerations

Morro Bay is a system under transition with a major eelgrass decline and recent trajectory of apparent eelgrass recovery. Studies have shown substantial daily and seasonal chemical variability in eelgrass dominated estuaries (Unsworth et al., 2012; Challener et al., 2016; Ricart et al., 2021). The major change in eelgrass that Morro Bay estuary has undergone may have altered its carbonate chemistry. Therefore, understanding carbonate chemistry in the bay during this period of low eelgrass presence provides a baseline for evaluating future change, as Morro Bay may be recovering with eelgrass acreage roughly tripling from 2017 (<6 ha) to 2019 (~15 ha) based on preliminary drone data (Walter and O'Leary, unpublished data). With eelgrass recovery, a smaller spatial gradient in carbonate chemistry may be expected between the forebay and the back bay due to increased photosynthesis decreasing DIC and increasing pH in the back bay in regions of recovery (Cyronak et al., 2018; Ricart et al., 2021). However, additional work is needed to understand the magnitude and timescales over which seagrass meadows can buffer seawater pH (Koweek et al., 2018), as amplification of diel pH signals in seagrass habitats are expected to increase with increasing anthropogenic CO_2, complicating the mitigation of low pH and saturation state on calcifying organisms (Pacella et al., 2018). In addition, pH variability is also controlled by TA, and TA levels depend on a variety of system properties (e.g. nutrient cycling, sediment dynamics, etc.), which are dynamic in nature. Moreover, the buffering ability of seagrass meadows is likely to be dependent on the hydrodynamics of the estuary (Cyronak et al., 2018). For example, the long water residence times in the back portions of Morro Bay may amplify the seagrass-induced changes to carbonate chemistry. Additionally, in shallow estuaries like Morro Bay, enhanced air-sea gas exchange may be a dominant driver of carbonate chemistry variability, both daily and seasonally. Therefore, if eelgrass recovers in Morro Bay, the data here will provide a unique opportunity to evaluate how changes in system ecology (e.g., aquatic habitat condition) interact with hydrodynamics to influence the carbonate chemistry system.

5. Conclusion

There is a growing need to understand the multiple drivers of carbonate chemistry in estuarine environments, particularly with the threat of climate change. This study found that the unique hydrodynamics (long flushing times and weak exchange) in LIEs moderate spatial gradients in carbonate chemistry. During the dry season in Morro Bay, we observed the highest temperature, salinity, TA, DIC, and pCO_2 and the lowest pH and Ω_A in the back bay relative to the bay mouth. Temperature, salinity, and TA increased at low tide while DIC and pH did not show large temporal variability with the exception of Late Summer. Increases in salinity contribute to a portion of TA and DIC changes but 67–80% of observed TA and 78–87% of DIC at low tide are likely driven by biogeochemical modifications accumulated during long flushing times. Although pH is consistently lower in the back portions of the bay, this area is likely being buffered from more extreme changes due to

elevated TA as a result of high flushing times. This potentially has important consequences for understanding estuarine buffering capacity and inorganic carbon cycling, and thus carbon storage potential of LIEs, as well as the chemical environments experienced by organisms in these ecosystems. At the same time, the hydrodynamics of LIEs are particularly sensitive to changes in climate and human disturbance (Largier et al., 1997; Schettini et al., 2017), which can further alter carbonate chemistry and lead to rapid ecosystem change. Therefore, managing LIEs sustainability into the future will require an understanding of how hydrodynamics and carbonate chemistry interact under different climate change scenarios. Additional studies that carefully monitor TA and DIC over time, and not solely pH, are necessary to fully constrain and understand the carbonate system, particularly in estuaries where TA and salinity are not strongly correlated as found in Morro Bay.

CRediT authorship contribution statement

Sarah E. Bartoloni: Writing – original draft, Visualization, Investigation. **Ryan K. Walter:** Writing – review & editing, Visualization, Funding acquisition, Conceptualization. **Sydney N. Wewerka:** Writing – review & editing, Visualization, Investigation. **Jolie Higgins:** Writing – review & editing, Investigation. **Jennifer K. O'Leary:** Writing – review & editing, Funding acquisition. **Emily E. Bockmon:** Writing – review & editing, Funding acquisition, Conceptualization.

Declaration of competing interest

The authors declare that they have no known competing financial interests or personal relationships that could have appeared to influence the work reported in this paper.

Data availability

Data is included in Supplementary Materials.

Acknowledgements

This publication was prepared under NOAA Grant #NA18OAR4170073, California Sea Grant College Program Project #R/HCE-07, through NOAA's National Sea Grant College Program, U.S. Department of Commerce. The statements, findings, conclusions and recommendations are those of the authors and do not necessarily reflect the views of California Sea Grant, NOAA, or the U.S. Dept. of Commerce. We also acknowledge the Cal Poly Research, Scholarly and Creative Activities Grant Program, supported by funds from the Provost's Office and the Chancellor's Office. Students were generously supported by the William and Linda Frost Fund. We also acknowledge support from the NOAA IOOS program through CeNCOOS. R. Walter and E. Bockmon were supported by the National Estuary Program-Coastal Watershed Grants from Restore America's Estuaries. We thank Ian Robbins, Jason Felton, and Tom Moylan for their help in the field and acknowledge Addie Norgaard, Garrett Schmid, Daniel Sandborn, and Nicholle Knopp for their role in sample collection and analysis. Boating resources were provided by the Cal Poly Center for Coastal Marine Sciences. We thank Ray Dienzo from the County of San Luis Obispo Public Works for assistance with the local stage height data.

Appendix A. Supplementary data

Supplementary data to this article can be found online at https://doi.org/10.1016/j.ecss.2022.108195.

References

Abe, H., Ito, M.A., Ahn, H., Nakaoka, M., 2022. Eelgrass beds can mitigate local acidification and reduce oyster malformation risk in a subarctic lagoon, Japan: a three dimensional ecosystem model study. Ocean Model. 173, 101992 https://doi.org/10.1016/j.ocemod.2022.101992.

Abril, G., Etcheber, H., Le Hir, P., Bassoullet, P., Boutier, B., Frankignoulle, M., 1999. Oxic/anoxic oscillations and organic carbon mineralization in an estuarine maximum turbidity zone (The Gironde, France). Limnol. Oceanogr. 44 (5), 1304–1315. https://doi.org/10.4319/lo.1999.44.5.1304.

Abril, G., Commarieu, M.-V., Maro, D., Fontugne, M., Guerin, F., Etcheber, H., 2004. A massive dissolved inorganic carbon release at spring tide in a highly turbid estuary. Geophys. Res. Lett. 31 https://doi.org/10.1029/2004GL019714.

Alin, S.R., Feely, R.A., Dickson, A.G., Martín Hernández-Ayón, J., Juranek, L.W., Ohman, M.D., Goericke, R., 2012. Robust empirical relationships for estimating the carbonate system in the southern California Current System and application to CalCOFI hydrographic cruise data (2005-2011). J. Geophys. Res.: Oceans 117 (5). https://doi.org/10.1029/2011JC007511.

Bates, N.R., Samuels, L., 2001. Biogeochemical and physical factors influencing seawater fCO2 and air-sea CO2 exchange on the Bermuda coral reef. Limnol. Oceanogr. 46 (4), 833–846. https://doi.org/10.4319/lo.2001.46.4.0833.

Bates, N.R., 2007. Interannual variability of the oceanic CO_2 sink in the subtropical gyre of the North Atlantic Ocean over the last 2 decades. J. Geophys. Res. 112 (C9) https://doi.org/10.1029/2006JC003759.

Baumann, H., Smith, E.M., 2018. Quantifying metabolically driven pH and oxygen fluctuations in US nearshore habitats at diel to interannual time scales. Estuar. Coast 41 (4), 1102–1117. https://doi.org/10.1007/s12237-017-0321-3.

Bockmon, E.E., Dickson, A.G., 2015. An inter-laboratory comparison assessing the quality of seawater carbon dioxide measurements. Mar. Chem. 171, 36–43. https://doi.org/10.1016/j.marchem.2015.02.002.

Borges, A.v., 2005. Do we have enough pieces of the jigsaw to integrate CO2 fluxes in the coastal ocean? Estuaries 28 (1), 3–27. https://doi.org/10.1007/BF02732750.

Borges, A. v, Gypens, N., 2010. Carbonate chemistry in the coastal zone responds more strongly to eutrophication than ocean acidification. Limnol. Oceanogr. 55 (1), 346–353. https://doi.org/10.4319/lo.2010.55.1.0346.

Bouillon, S., Middelburg, J.J., Dehairs, F., Borges, A. v, Abril, G., Flindt, M.R., Ulomi, S., Kristensen, E., 2007. Importance of intertidal sediment processes and porewater exchange on the water column biogeochemistry in a pristine mangrove creek (Ras Dege, Tanzania). Biogeosciences 4 (3), 311–322. https://doi.org/10.5194/bg-4-311-2007.

Brodeur, J.R., Chen, B., Su, J., Xu, Y.Y., Hussain, N., Scaboo, M.M., Zhang, Y., Testa, J. M., Cai, W.J., 2019. Chesapeake bay inorganic carbon: spatial distribution and seasonal variability. Front. Mar. Sci. 6 https://doi.org/10.3389/fmars.2019.00099.

Buck, C.M., Wilkerson, F.P., Parker, A.E., Dugdale, R.C., 2014. The influence of coastal nutrients on phytoplankton productivity in a shallow low inflow estuary, drakes estero, California (USA). Estuar. Coast 37 (4), 847–863. https://doi.org/10.1007/s12237-013-9737-6.

Cai, W.-J., Wang, Y., 1998. The chemistry, fluxes, and sources of carbon dioxide in the estuarine waters of the Satilla and Altamaha Rivers, Georgia. Limnol. Oceanogr. 43 (4), 657–668. https://doi.org/10.4319/lo.1998.43.4.0657.

Cai, W.-J., Huang, W.-J., Luther, G.W., Pierrot, D., Li, M., Testa, J., Xue, M., Joesoef, A., Mann, R., Brodeur, J., Xu, Y.-Y., Chen, B., Hussain, N., Waldbusser, G.G., Cornwell, J., Kemp, W.M., 2017. Redox reactions and weak buffering capacity lead to acidification in the Chesapeake Bay. Nat. Commun. 8, 369. https://doi.org/10.1038/s41467-017-00417-7.

Cai, W.-J., Feely, R.A., Testa, J.M., Li, M., Evans, W., Alin, S.R., Xu, Y.-Y., Pelletier, G., Ahmed, A., Greeley, D.J., Newton, J.A., Bednaršek, N., 2020. Natural and anthropogenic drivers of acidification in large estuaries. Ann. Rev. Mar. Sci 19, 1–19. https://doi.org/10.1146/annurev-marine-010419, 33.

Cantoni, C., Luchetta, A., Celio, M., Cozzi, S., Raicich, F., Catalano, G., 2012. Carbonate system variability in the gulf of trieste (north adriatic sea). Estuar. Coast Shelf Sci. 115, 51–62. https://doi.org/10.1016/j.ecss.2012.07.006.

Carstensen, J., Chierici, M., Gustafsson, B.G., Gustafsson, E., 2018. Long-term and seasonal trends in estuarine and coastal carbonate systems. Global Biogeochem. Cycles 32 (3), 497–513. https://doi.org/10.1002/2017GB005781.

Challener, R.C., Robbins, L.L., Mcclintock, J.B., 2016. Variability of the carbonate chemistry in a shallow, seagrass-dominated ecosystem: implications for ocean acidification experiments. Mar. Freshw. Res. 67 (2), 163–172. https://doi.org/10.1071/MF14219.

Cotovicz, L.C., Knoppers, B.A., Brandini, N., Costa Santos, S.J., Abril, G., 2015. A Strong CO2 sink enhanced by eutrophication in a tropical coastal embayment (Guanabara Bay, Rio de Janeiro, Brazil). Biogeosciences 12, 6125–6146. https://doi.org/10.5194/bg-12-6125-2015.

Cotovicz, L.C., Knoppers, B., Régis, C., Tremmel, D., Costa-Santos, S., Abril, G., 2021. Eutrophication overcoming carbonate precipitation in a tropical hypersaline coastal lagoon acting as a CO2 sink (Araruama Lagoon, SE Brazil). Biogeochemistry 156, 231–254. https://doi.org/10.1007/s10533-021-00842-3. Springer Verlag.

Cotovicz, L.C., Marins, R.V., da Silva, A.R., 2022. Eutrophication amplifies the diel variability of carbonate chemistry in an equatorial, semi-arid, and negative estuary. Front. Mar. Sci. 9 https://doi.org/10.3389/fmars.2022.767632.

Crosswell, J.R., Carlin, G., Steven, A., 2020. Controls on carbon, nutrient, and sediment cycling in a large, semiarid estuarine system; princess charlotte bay, Australia. J. Geophys. Res.: Biogeosciences 125 (1). https://doi.org/10.1029/2019JG005049.

Cyronak, T., Santos, I.R., Erler, D.V., Eyre, B.D., 2013. Groundwater and porewater as major sources of alkalinity to a fringing coral reef lagoon (Muri Lagoon, Cook Islands). Biogeosciences 10, 2467–2480. https://doi.org/10.5194/bg-10-2467-2013.

Cyronak, T., Andersson, A.J., D'Angelo, S., Bresnahan, P., Davidson, C., Griffin, A., Kindeberg, T., Pennise, J., Takeshita, Y., White, M., 2018. Short-term spatial and temporal carbonate chemistry variability in two contrasting seagrass meadows:

implications for pH buffering capacities. Estuar. Coast 41 (5), 1282–1296. https://doi.org/10.1007/s12237-017-0356-5.
Dore, J.E., Lukas, R., Sadler, D.W., Church, M.J., Karl, D.M., 2009. Physical and biogeochemical modulation of ocean acidification in the central North Pacific. Proc. Natl. Acad. Sci. USA 106 (30), 12235–12240. https://doi.org/10.1073/pnas.0906044106.
Dickson, A.G., 1990. Standard potential of the reaction: AgCl(s) + 1/2 H_2(g) = Ag(s) + HCl(aq), and the standard acidity constant of the ion HSO_4^- in synthetic seawater from 273.15 to 318.15 K. J. Chem. Thermodyn. 22 (2), 113–127. https://doi.org/10.1016/0021-9614(90)90074-Z.
Dickson, A.G., Afghan, J.D., Anderson, G.C., 2003. Reference materials for oceanic CO2 analysis: a method for the certification of total alkalinity. Mar. Chem. 80, 185–197. https://doi.org/10.1016/S0304-4203(02)00133-0.
Dickson, A.G., Sabine, C.L., Christian, J.R., 2007. Guide to Best Practices for Ocean CO2 Measurements.
Duarte, C.M., Marba, N., Gacia, E., Fourqurean, J.W., Beggins, J., Barron, C., Apostolaki, E.T., 2010. Seagrass community metabolism: assessing the carbon sink capacity of seagrass meadows. Global Biogeochem. Cycles 24 (4). https://doi.org/10.1029/2010GB003793.
Feely, R.A., Alin, S.R., Newton, J., Sabine, C.L., Warner, M., Devol, A., Krembs, C., Maloy, C., 2010. The combined effects of ocean acidification, mixing, and respiration on pH and carbonate saturation in an urbanized estuary. Estuar. Coast Shelf Sci. 88 (4), 442–449. https://doi.org/10.1016/j.ecss.2010.05.004.
Feely, R.A., Sabine, C.L., Byrne, R.H., Millero, R.J., Dickson, A.G., Wanninkhof, R., Murata, A., Miller, L.A., Greeley, D., 2012. Decadal changes in the aragonite and calcite saturation state of the Pacific Ocean. Global Biogeochem. Cycles 26 (3). https://doi.org/10.1029/2011GB004157.
Fong, M.B., Dickson, A.G., 2019. Insights from GO-SHIP hydrography data into the thermodynamic consistency of CO2 system measurements in seawater. Mar. Chem. 211 (January), 52–63. https://doi.org/10.1016/j.marchem.2019.03.006.
Frankignoulle, M., Abril, G., Borges, A., Bourge, I., Canon, C., Delille, B., Libert, E., Théate, J.M., 1998. Carbon dioxide emission from European estuaries. Science 282 (5388), 434–436. https://doi.org/10.1126/science.282.5388.434.
Gruber, N., Hauri, C., Lachkar, Z., Loher, D., Frölicher, T.L., Plattner, G.K., 2012. Rapid progression of ocean acidification in the California Current System. Science 337 (6091), 220–223. https://doi.org/10.1126/science.1216773.
Hall-Spencer, J.M., Harvey, B.P., 2019. Ocean acidification impacts on coastal ecosystem services due to habitat degradation. Emerging Topics in Life Sciences 3 (2), 197–206. https://doi.org/10.1042/ETLS20180117. Portland Press Ltd.
Hauri, C., Gruber, N., Plattner, G.-K., Alin, S., Feely, R.A., Hales, B., Wheeler, P.A., 2009. ocean acidification in the California current system. Oceanography 22 (4), 60–71. Retrieved from. http://www.jstor.org/stable/24861024.
Hendriks, I.E., Olsen, Y.S., Ramajo, L., Basso, L., Steckbauer, A., Morre, T.S., Howard, J., Duarte, C.M., 2014. Photosynthetic activity buffers ocean acidification in seagrass meadows. Biogeosciences 11, 333–346. https://doi.org/10.5194/bg-11-333-2014.
Hofmann, G.E., Smith, J.E., Johnson, K.S., Send, U., Levin, L.A., Micheli, F., Paytan, A., Price, N.N., Peterson, B., Takeshita, Y., Matson, P.G., Crook, E.D., Kroeker, K.J., Gambi, M.C., Riivest, E.B., Frieder, C.A., Yu, P.C., Martz, T.R., 2011. High-frequency dynamics of ocean pH: a multi-ecosystem comparison. PLoS One 6 (12). https://doi.org/10.1371/journal.pone.0028983.
Hu, X., Pollack, J.B., McCutcheon, M.R., Montagna, P.A., Ouyang, Z., 2015. Long-term alkalinity decrease and acidification of estuaries in northwestern gulf of Mexico. Environ. Sci. Technol. 49 (6), 3401–3409. https://doi.org/10.1021/es505945p.
Jiang, L.-Q., Cai, W.-J., Wang, Y., 2008. A comparative study of carbon dioxide degassing in river- and marine-dominated estuaries. Limnol. Oceanogr. 53 (6), 2603–2615. https://doi.org/10.1021/es505945p.
Jiang, Z.P., Tyrrell, T., Hydes, D.J., Dai, M., Hartman, S.E., 2014. Variability of alkalinity and the alkalinity-salinity relationship in the tropical and subtropical surface ocean. Global Biogeochem. Cycles 28 (7), 729–742. https://doi.org/10.1002/2013GB004678.
Jiang, L.-Q., Carter, B.R., Feely, R.A., Lauvset, S.K., Olsen, A., 2019. Surface ocean pH and buffering capacity: past, present, and future. Nature Scientific Reports 9, 18624. https://doi.org/10.1038/s41598-019-55039-4.
Kemp, W.M., Boynton, W.R., Adolf, J.E., Boesch, D.F., Boicourt, W.C., Brush, G., Cornwell, J., Fisher, T., Gilbert, P., hagy, J., Harding, L., Houde, E., Kimmel, D., Miller, W.D., Newell, R., Roman, M.R., Smith, E.M., Stevenson, J.C., 2005. Eutrophication of Chesapeake Bay: historical trends and ecological interactions. Marine Ecology Progress Series Mar Ecol Prog Ser 303, 1–29. https://doi.org/10.3354/MEPS303001.
Kerr, D.E., Brown, P.J., Grey, A., Kelleher, B.P., 2021. The influence of organic alkalinity on the carbonate system in coastal waters. Mar. Chem. 237 https://doi.org/10.1016/j.marchem.2021.104050.
Koweek, D.A., Zimmerman, R.C., Hewett, K.M., Gaylord, B., Giddings, S.N., Nickols, K.J., Ruesink, J.L., Stachowicz, J.J., Takeshita, Y., Caldeira, K., 2018. Expected limits on the ocean acidification buffering potential of a temperate seagrass meadow. Ecol. Appl. 28 (7), 1694–1714. https://doi.org/10.1002/eap.1771.
Kroeker, K.J., Kordas, R.L., Crim, R., Hendriks, I.E., Ramajo, L., Singh, G.S., Duarte, C.M., Gattuso, J.P., 2013. Impacts of ocean acidification on marine organisms: quantifying sensitivities and interaction with warming. Global Change Biol. 19 (6), 1884–1896. https://doi.org/10.1111/gcb.12179.
Krumins, V., Gehlen, M., Arndt, S., van Cappellen, P., Regnier, P., 2013. Dissolved inorganic carbon and alkalinity fluxes from coastal marine sediments: model estimates for different shelf environments and sensitivity to global change. Biogeosciences 10 (1), 371–398. https://doi.org/10.5194/bg-10-371-2013.
Largier, J., 2010. Low-inflow estuaries: hypersaline, inverse, and thermal scenarios. In: Valle-Levinson, A. (Ed.), Contemporary Issues in Estuarine Physics. Cambridge University Press, Cambridge. https://doi.org/10.1017/CBO9780511676567.010.
Largier, J.L., Hollibaugh, J.T., Smith, S.v., 1997. Seasonally hypersaline estuaries in mediterranean-climate regions. Estuar. Coast Shelf Sci. 45 https://doi.org/10.1006/ecss.1997.0279.
Lee, K., Kim, T.-W., Byrne, R.H., Millero, F.J., Feely, R.A., Liu, Y.-M., 2010. The universal ratio of boron to chlorinity for the North Pacific and North Atlantic oceans. Geochem. Cosmochim. Acta 74 (6). https://doi.org/10.1016/j.gca.2009.12.027, 1901-1811.
Li, M., Lee, Y.J., Testa, J.M., Li, Y., Ni, W., Kemp, W.M., di Toro, D.M., 2016. What drives interannual variability of hypoxia in Chesapeake Bay: climate forcing versus nutrient loading? Geophys. Res. Lett. 43, 2127–2134. https://doi.org/10.1002/2015GL067334.
Liu, Q., Charette, M.A., Breier, C.F., Henderson, P.B., McCorkle, D.C., Martin, W., Dai, M., 2017. Carbonate system biogeochemistry in a subterranean estuary – waquoit Bay, USA. Geochem. Cosmochim. Acta 203, 422–439. https://doi.org/10.1016/j.gca.2017.01.041.
Li, M., Li, R., Cai, W.-J., Testa, J.M., Shen, C., 2020. Effects of wind-driven lateral upwelling on estuarine carbonate chemistry. Front. Mar. Sci. 7 (588465) https://doi.org/10.3389/fmars.2020.588465.
Lukawska-Matuszewska, K., Grzybowski, W., Szewczun, A., Tarasiewicz, P., 2018. Constituents of organic alkalinity in pore water of marine sediments. Mar. Chem. 200, 22–32. https://doi.org/10.1016/j.marchem.2018.01.012.
Malone, T.C., Newton, A., 2020. The globalization of cultural eutrophication in the coastal ocean: causes and consequences. Front. Mar. Sci. 7, 670. https://doi.org/10.3389/fmars.2020.00670. Frontiers Media S.A.
McCutcheon, M.R., Staryk, C.J., Hu, X., 2019. Characteristics of the carbonate system in a semiarid estuary that experiences summertime hypoxia. Estuar. Coast 42 (6), 1509–1523. https://doi.org/10.1007/s12237-019-00588-0.
McGrath, T., McGovern, E., Cave, R.R., Kivimäe, C., 2016. The inorganic carbon chemistry in coastal and shelf waters around Ireland. Estuar. Coast 39, 27–39. https://doi.org/10.1007/s12237-015-9950-6.
Miller, A.W., Reynolds, A.C., Sobrino, C., Riedel, G.F., 2009. Shellfish face uncertain future in high CO2 world: influence of acidification on oyster larvae calcification and growth in estuaries. PLoS One 4 (5). https://doi.org/10.1371/journal.pone.0005661.
Millero, F.J., 2010. Carbonate constants for estuarine waters. Mar. Freshw. Res. 61 (2), 139–142. https://doi.org/10.1071/MF09254.
Murgulet, D., Trevino, M., Douglas, A., Spalt, N., Hu, X., Murgulet, V., 2018. Temporal and spatial fluctuations of groundwater-derived alkalinity fluxes to a semiarid coastal embayment. Sci. Total Environ. 630, 1343–1359. https://doi.org/10.1016/j.scitotenv.2018.02.333.
Nidzieko, N.J., Monismith, S.G., 2013. Contrasting seasonal and fortnightly variations in the circulation of a seasonally inverse estuary, elkhorn slough, California. Estuar. Coast 36 (1), 1–17. https://doi.org/10.1007/s12237-012-9548-1.
Olafsson, J., Olafsdottir, S.R., Benoit-Cattin, A., Takahashi, T., 2010. The Irminger Sea and the Iceland Sea time series measurements of sea water carbon and nutrient chemistry 1983-2008. Earth Syst. Sci. Data 2, 99–104. https://doi.org/10.3334/CDIAC/otg.CARINA.AMS.V1.2.
O'Leary, J.K., Goodman, M.C., Walter, R.K., Willits, K., Pondella, D.J., Stephens, J., 2021. Effects of estuary-wide seagrass loss on fish populations. Estuar. Coast. https://doi.org/10.1007/s12237-021-00917-2.
Omarjee, A., Taljaard, S., Weerts, S.P., Adams, J.B., 2020. The influence of mouth status on pH variability in small temporarily closed estuaries. Estuar. Coast Shelf Sci. 246 https://doi.org/10.1016/j.ecss.2020.107043.
Pacella, S.R., Brown, C.A., Waldbusser, G.G., Labiosa, R.G., Hales, B., Karl, D.M., 2018. Seagrass habitat metabolism increases short-term extremes and long-term offset of CO2 under future ocean acidification. Proc. Natl. Acad. Sci. USA 115 (15), 3870–3875. https://doi.org/10.23719/1407616.
Paulsen, M.L., Andersson, A.J., Aluwihare, L., Cyronak, T., D'Angelo, S., Davidson, C., Elwany, H., Giddings, S.N., Page, H.N., Porrachia, M., Schroeter, S., 2018. Temporal changes in seawater carbonate chemistry and carbon export from a southern California estuary. Estuar. Coast 41 (4), 1050–1068. https://doi.org/10.1007/s12237-017-0345-8.
Reum, J.C.P., Alin, S.R., Feely, R.A., Newton, J., Warner, M., McElhany, P., 2014. Seasonal carbonate chemistry covariation with temperature, oxygen, and salinity in a fjord estuary: implications for the design of ocean acidification experiments. PLoS One 9 (2). https://doi.org/10.1371/journal.pone.0089619.
Ricart, A.M., Ward, M., Hill, T.M., Scanford, E., Kroeker, K.J., Takeshita, Y., Merolla, S., Shukla, P., Ninokawa, A.T., Elsmore, K., Gaylord, B., 2021. Coast-wide evidence of low pH amelioration by seagrass ecosystems. Global Change Biol. 27 (11), 2580–2591. https://doi.org/10.1111/gcb.15594.
Rosenfeld, L.K., Schwing, F.B., Garfield, N., Tracy, D.E., 1994. Birfurcated flow from an upwelling center: a cold water source for Monterey Bay. Continent. Shelf Res. 14 (9), 931–964. https://doi.org/10.1016/0278-4343(94)90058-2.
Santana-Casiano, M.J., Gonzalez-Davila, M., Rueda, M.-J., Llinas, O., Gonzalez-Davila, E.-F., 2007. The interannual variability of oceanic CO_2 parameters in the northeast Atlantic subtropical gyre at the ESTOC site. Global Biogeochem. Cycles 21 (1). https://doi.org/10.1029/2006GB002788.
Schettini, C.A.F., Valle-Levinson, A., Truccolo, E.C., 2017. Circulation and transport in short, low-inflow estuaries under anthropogenic stresses. Regional Studies in Marine Science 10. https://doi.org/10.1016/j.rsma.2017.01.004.
Shen, C., Testa, J.M., Li, M., Cai, W., 2020. Understanding anthropogenic impacts on pH and aragonite saturation state in Chesapeake bay: insights from a 30-year model

study. J. Geophys. Res.: Biogeosciences 125 (7). https://doi.org/10.1029/2019JG005620.

Shen, C., Testa, J.M., Li, M., Cai, W.J., Waldbusser, G.G., Ni, W., Kemp, M., Cornwell, J., Chen, B., Brodeur, J., Su, J., 2019. Controls on carbonate system dynamics in a coastal plain estuary: a modeling study. J. Geophys. Res.: Biogeosciences 124 (1), 61–78. https://doi.org/10.1029/2018JG004802.

Sippo, J.Z., Maher, D.T., Tait, D.R., Holloway, C., Santos, I.R., 2016. Are mangroves drivers or buffers of coastal acidification? Insights from alkalinity and dissolved inorganic carbon export estimates across a latitudinal transect. Global Biogeochem. Cycles 30 (5), 753–766. https://doi.org/10.1002/2015GB005324.

Song, S., Wang, Z.A., Gonneea, M.E., Kroeger, K.D., Chu, S.N., Li, D., Liang, H., 2020. An important biogeochemical link between organic and inorganic carbon cycling: effects of organic alkalinity on carbonate chemistry in coastal waters influenced by intertidal salt marshes. Geochem. Cosmochim. Acta 275, 123–139. https://doi.org/10.1016/j.gca.2020.02.013.

Suanda, S.H., Barth, J.A., Woodson, C.B., 2011. Diurnal heat balance for the northern Monterey Bay inner shelf. Journal of Geophysical Research Oceans 116 (C9). https://doi.org/10.1029/2010JC006894.

Unsworth, R.K.F., Collier, C.J., Henderson, G.M., McKenzie, L.J., 2012. Tropical seagrass meadows modify seawater carbon chemistry: implications for coral reefs impacted by ocean acidification. Environ. Res. Lett. 7 (2) https://doi.org/10.1088/1748-9326/7/2/024026.

van Heuven, S., Pierrot, D., Rae, J.W.B., Lewis, E., Wallace, D.W.R., 2011. ATLAB Program Developed for CO2 System Calculations. Tennessee: Carbon Dioxide Information Analysis Center, Oak Ridge National Laboratory, U.S. Department of Energy, Oak Ridge. https://doi.org/10.3334/CDIAC/otg.CO2SYS_MATLAB_v1.1.

Wallace, R.B., Baumann, H., Grear, J.S., Aller, R.C., Gobler, C.J., 2014. Coastal ocean acidification: the other eutrophication problem. Estuar. Coast Shelf Sci. 148, 1–13. https://doi.org/10.1016/j.ecss.2014.05.027.

Walter, R.K., Reid, E.C., Davis, K.A., Armenta, K.J., Merhoff, K., Nidzieko, N.J., 2017. Local diurnal wind-driven variability and upwelling in a small coastal embayment. Journal of Geophysical Research Oceans 122 (2), 955–972. https://doi.org/10.1002/2016JC012466.

Walter, R.K., Rainville, E.J., O'Leary, J.K., 2018a. Hydrodynamics in a shallow seasonally low-inflow estuary following eelgrass collapse. Estuar. Coast Shelf Sci. 213, 160–175. https://doi.org/10.1016/j.ecss.2018.08.026.

Walter, R.K., Armenta, K.J., Shearer, B., Robbins, I., Steinbeck, J., 2018b. Coastal upwelling seasonality and variability of temperature and chlorophyll in a small coastal embayment. Continent. Shelf Res. 154, 9–18. https://doi.org/10.1016/j.csr.2018.01.002.

Walter, R.K., O'Leary, J.K., Vitousek, S., Taherkhani, M., Geraghty, C., Kitajima, A., 2020. Large-scale erosion driven by intertidal eelgrass loss in an estuarine environment. Estuar. Coast Shelf Sci. 243 https://doi.org/10.1016/j.ecss.2020.106910.

Wolf-Gladrow, D.A., Zeebe, R.E., Klaas, C., Körtzinger, A., Dickson, A.G., 2007. Total alkalinity: the explicit conservative expression and its application to biogeochemical processes. Mar. Chem. 106 (1–2), 287–300. https://doi.org/10.1016/j.marchem.2007.01.006.

Worm, B., Barbier, E.B., Beaumont, N., Duffy, J.E., Folke, C., Halpern, B.S., Jackson, J.B. C., Lotze, H.K., Micheli, F., Palumbi, S.R., Sala, E., Selkoe, K.A., Stachowicz, J.J., Watson, R., 2006. Impacts of biodiversity loss on ocean ecosystem services. Science 314 (5800), 787–790. https://doi.org/10.1126/science.1132294.

Yao, H., Hu, X., 2017. Responses of carbonate system and CO2 flux to extended drought and intense flooding in a semiarid subtropical estuary. Limnol. Oceanogr. 62, S112–S130. https://doi.org/10.1002/lno.10646.